Cancer Therapy: Preclinical

Clinical Cancer Research

Integrated Pharmacokinetic/Pharmacodynamic Model of a Bispecific CD3xCD123 DART Molecule in Nonhuman Primates: Evaluation of Activity and Impact of Immunogenicity

Olivia Campagne[1,2,3], Audrey Delmas[1], Sylvain Fouliard[1], Marylore Chenel[1], Gurunadh R. Chichili[4], Hua Li[4], Ralph Alderson[4], Jean-Michel Scherrmann[2], and Donald E. Mager[3]

Abstract

Purpose: Flotetuzumab (MGD006 or S80880) is a bispecific molecule that recognizes CD3 and CD123 membrane proteins, redirecting T cells to kill CD123-expressing cells for the treatment of acute myeloid leukemia. In this study, we developed a mathematical model to characterize MGD006 exposure–response relationships and to assess the impact of its immunogenicity in cynomolgus monkeys.

Experimental Design: Thirty-two animals received multiple escalating doses (100-300-600-1,000 ng/kg/day) via intravenous infusion continuously 4 days a week. The model reflects sequential binding of MGD006 to CD3 and CD123 receptors. Formation of the MGD006/CD3 complex was connected to total T cells undergoing trafficking, whereas the formation of the trimolecular complex results in T-cell activation and clonal expansion. Activated T cells were used to drive the peripheral depletion of CD123-positive cells. Anti-drug antibody development was linked to MGD006 disposition as an elimination pathway. Model validation was tested by predicting the activity of MGD006 in eight monkeys receiving continuous 7-day infusions.

Results: MGD006 disposition and total T-cell and CD123-positive cell profiles were well characterized. Anti-drug antibody development led to the suppression of T-cell trafficking but did not systematically abolish CD123-positive cell depletion. Target cell depletion could persist after drug elimination owing to the self-proliferation of activated T cells generated during the first cycles. The model was externally validated with the 7-day infusion dosing schedule.

Conclusions: A translational model was developed for MGD006 that features T-cell activation and expansion as a key driver of pharmacologic activity and provides a mechanistic quantitative platform to inform dosing strategies in ongoing clinical studies. *Clin Cancer Res; 24(11); 2631–41. ©2018 AACR.*

Introduction

Acute myeloid leukemia (AML) results from the rapid proliferation and accumulation of abnormal immature myeloid cells (blasts) in the bone marrow. The blasts interfere with normal hematopoiesis leading to bone marrow failure, blood invasion, and infiltration of several organs, including brain and lung (1). AML is uncommon in individuals under the age of 45 years, with a median age at diagnosis of 67 years. Current treatments include standard induction chemotherapy, with treatment strategies based on the age and prognosis of the patient (2, 3). Despite many attempts for new drugs and combinations, treatment has changed little in the last 30 years, and the current 5-year survival rate is approximately 26% (4). AML represents a diverse classification, as the disease is highly phenotypically and genetically heterogeneous, which significantly adds to the challenge of developing new efficient treatments (1, 5).

Among the emerging compounds for the treatment of hematologic malignancies, bispecific T-cell antibodies, which rely on immune-mediated mechanisms, represent a promising approach (6). Bispecific antibodies are not new (7); however, improvements in engineering have renewed interest in this antibody construct, and there are multiple bispecific agents in clinical development (8). In addition, blinatumomab, a bispecific T-cell engager (BiTE) CD3xCD19 targeting antibody, received an accelerated approval by the FDA for the treatment of a rare form of acute lymphoblastic leukemia (9). Bispecific biotherapeutics bind to both CD3, a T-cell receptor (10), and a target antigen expressed on cancer cells, to recruit and redirect patient T lymphocytes to tumor cells for elimination. The binding of drug to both the receptor and antigen leads to the formation of a cytolytic immunologic synapse. This is followed by polyclonal T-cell activation and proliferation, independent of T-cell receptor specificity, peptide antigen presentation, or costimulatory signals (11–13). Depletion of target cells occurs by the release of cytokines from activated T cells and lytic granules in the synapse.

[1]Clinical Pharmacokinetics and Pharmacometrics, Institut de Recherches Internationales Servier, Suresnes, France. [2]INSERM UMR-S-1144, Universités Paris Descartes-Paris Diderot, Paris, France. [3]Department of Pharmaceutical Sciences, University at Buffalo, State University of New York, Buffalo, New York. [4]MacroGenics, Inc., Rockville, Maryland.

Note: Supplementary data for this article are available at Clinical Cancer Research Online (http://clincancerres.aacrjournals.org/).

Corresponding Author: Donald E. Mager, University at Buffalo, State University of New York, 431 Kapoor Hall, Buffalo, NY 14214-8033. Phone: 716-645-2903; Fax: 716-645-3693; E-mail: dmager@buffalo.edu

doi: 10.1158/1078-0432.CCR-17-2265

Translational Relevance

Bispecific antibodies that redirect T cells to kill target antigen-expressing cells represent a promising approach for treating cancer. However, the stoichiometry required for optimal efficacy among the drug, T cells, and the target ligand is not well understood. A pharmacokinetic/pharmacodynamic model was developed for a bispecific CD3xCD123 DART molecule, under development for the treatment of acute myeloid leukemia, in cynomolgus monkeys. The model simultaneously describes antibody binding to both peripheral CD3-expressing T cells and CD123-positive cells, T-cell trafficking, activation, and expansion, and the peripheral depletion of CD123-positive cells, along with the impact of anti-drug antibody formation. The model provides key insights into the dynamic interplay among system components regulating drug action. By integrating primary pharmacokinetic and pharmacological processes, the model represents an efficient translational framework to provide quantitative predictions of drug disposition and potency in humans, and to anticipate dosing strategies to inform ongoing clinical trials.

The Dual-Affinity Re-Targeting (DART) technology is a bispecific antibody platform, the format of which is similar to BiTE molecules, but with improved stability and manufacturability and a greater potency as compared with blinatumomab (14). Flotetuzumab (MGD006 or S80880) is a CD3xCD123 DART protein designed to target CD123-positive cells for elimination by CD3-expressing T cells. CD123, or IL3 receptor α chain, is a membrane protein that represents a potential therapeutic target in several hematologic malignancies, including AML (15, 16). CD123 is overexpressed on leukemia stem cells of patients with AML and is expressed in blasts of most patients. CD123 expression does not vary by AML subtype and has been correlated with tumor burden and poor prognosis (16). The protein is also normally expressed on some blood cells, such as plasmacytoid dendritic cells or monocytes, and by a subset of normal myeloid progenitors, but little to no expression on normal hematopoietic stem cells. This supports the CD123-targeting approach, as normal hematopoiesis could be reconstituted after $CD123^+$ cell depletion.

The ability of MGD006 to induce T-cell–mediated $CD123^+$ cell depletion has been shown *in vitro* and in mouse models, with efficacy correlating with CD123 expression (17, 18). In toxicology studies in cynomolgus monkeys (a cross-reactive species), MGD006 displayed favorable pharmacodynamic activity with near complete depletion of circulating normal $CD123^+$-cells and a good safety profile. However, anti-drug antibodies were developed in 70% of the animals (17). Similar to blinatumomab, MGD006 results in circulating T-lymphocyte cell trafficking, which may be triggered by monovalent binding of the compound to CD3 (19). The objectives of this study were to (i) develop a pharmacokinetic model for MGD006 disposition in monkeys, (ii) develop pharmacodynamic models to link MGD006 exposure with T-cell trafficking and $CD123^+$ cell depletion, and (iii) evaluate the impact of ADA development on these outcomes. A population modeling approach was used to characterize the variability of the pharmacokinetic and pharmacodynamic parameters across the animals. The final pharmacokinetic/pharmacodynamic model aims to integrate mechanisms of action of the bispecific antibody to inform dosing strategies in ongoing clinical trials.

Materials and Methods

Preclinical experimental design

This nonhuman primate study was performed at Charles River Laboratories, according to the guidelines of their Institutional Animal Care and Use Committee (IACUC; ref. 17). Treatment-naïve cynomolgus monkeys (*Macaca fascicularis*) of Chinese origin (weight range: 2.7–5 kg) were randomly assigned to six groups (four males and four females per group). Animals were treated on a weekly basis for 5 weeks with vehicle control or MGD006 administrated intravenously as a 4-day (groups 1–5) or 7-day (group 6) continuous infusion through infusion pumps (CADD-Legacy, SIMS Deltec Inc.). One vehicle control and four escalating MGD006 dose levels were administrated to groups 2–6 (100-300-600-1,000 ng/kg/day), whereas group 1 only received the vehicle control. More details are provided in Supplementary Fig. S1.

Bioanalysis

Serum samples (2 mL) were taken at predose on day 1 and after each infusion. Additional samples were collected at predose, 4 and 24 hours after the start of infusion, and 0.25, 1, 3, 8, 24, and 48 hours after the end of infusion for group 3 (third week) and group 4 (fourth week). Free MGD006 concentrations were measured using a validated sandwich immunoassay with electrochemiluminescence detection (Meso Scale Diagnostics) and a limit of quantification (LOQ) of 10 pg/mL.

A validated bridging ELISA was used to detect and confirm the presence of ADA in serum samples before the start of each infusion and during the recovery period at days 36, 44, and 65. ADA development was reported as either positive or negative. The assay limit of detection (LOD) was 25 ng/mL for anti-MGD006 antibodies in the presence of up to 100 ng/mL of MGD006.

FACS analysis of monkey whole blood samples was performed with a LSRFortessa analyser (BD Biosciences) to monitor the number of total CD3 T cells and $CD123^+$ peripheral cells. For FACS analysis, 1.25 mL of whole blood was obtained at predose and 72 hours after the start of each infusion and during the recovery period at days 36, 44, 51, 58, and 65. The absolute number of cells was determined with TruCOUNT (BD Biosciences).

Model development

A mathematical model based on a series of ordinary differential equations was developed to describe MGD006 disposition, the effect of its immunogenicity, and the dynamics of T cells and $CD123^+$ cells. A simplified representation of the final pharmacokinetic/pharmacodynamic model is shown in Fig. 1, and a more detailed structural model is provided in Supplementary Materials (Supplementary Fig. S2). Key equations are provided here, and the complete set of equations is listed in Supplementary Materials (Supplementary Section S1).

Formation of the trimolecular synapse. Molar concentrations of each receptor (RT_t) were calculated on the basis of the absolute count (N cells/L) of the cells expressing the receptor (T cells or

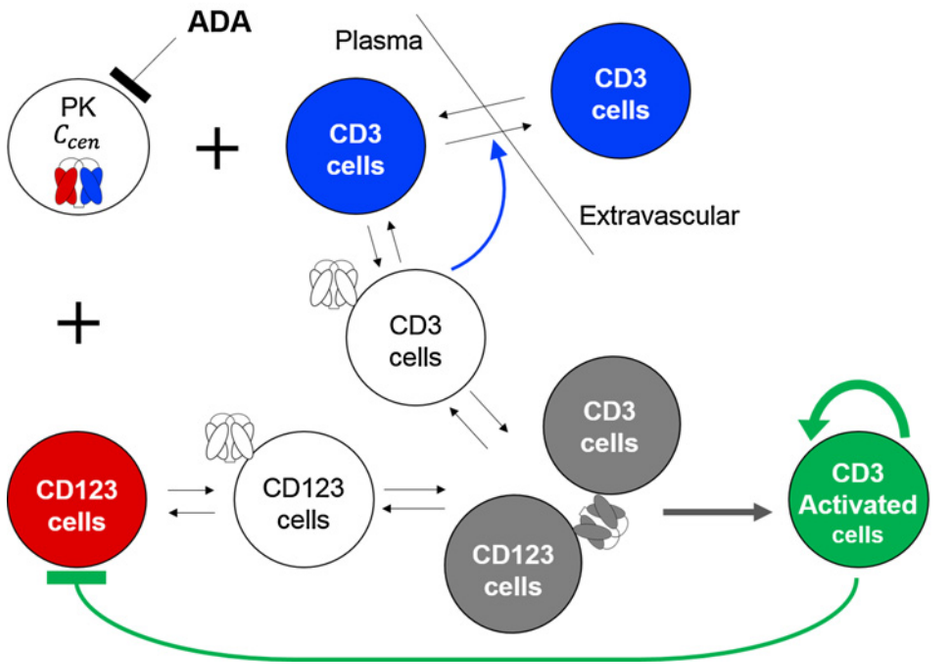

Figure 1.
Mechanistic pharmacokinetic/pharmacokinetic model for MGD006 administrated to cynomolgus monkeys. Pharmacokinetic functions describe free MGD006 plasma concentrations inhibited by anti-drug antibodies (ADA, black line). MGD006 binds in a sequential manner to CD3 and CD123 proteins. The MGD006/CD3 complex leads to T-cell redistribution (blue arrow). The trimolecular complex leads to T-cell activation and expansion (gray and green arrow), which drive the peripheral depletion of CD123 cells (green line). Supplementary Fig. S2 provides the structural model.

$CD123^+$ cells) and the receptor density (RT_d) as follows:

$$RT_t = \frac{RT_d \cdot N}{N_A} \tag{1}$$

where N_A is Avogadro's constant. Both numbers of receptors produced by each cell were assumed to be constant over time and fixed to 60,000 and 25,000 receptors/cell for $CD3^+$ and $CD123^+$ cells (20, 21). Formation of the synapse was modeled as a sequential binding process between unbound molar drug, CD3, and CD123 concentrations (Fig. 1). It was assumed that the bimolecular complexes MGD006/CD3 (DTC) and MGD006/CD123 (DTA), and the trimolecular complex (SYN) were eliminated from plasma only by dissociation of the complex. The following equations describe the formation of the three complexes:

$$\begin{aligned}\frac{dDTC}{dt} = {} & k_{on-TC} \cdot C_{cen} \cdot RTC_u - k_{off-TC} \\ & \cdot DTC - k_{on-TA} \cdot DTC \cdot RTA_u \\ & + k_{off-TA} \cdot SYN; \qquad DTC(0) = 0\end{aligned} \tag{2}$$

$$\begin{aligned}\frac{dDTA}{dt} = {} & k_{on-TA} \cdot C_{cen} \cdot RTA_u - k_{off-TA} \cdot DTA - k_{on-TC} \\ & \cdot DTA \cdot RTC_u + k_{off-TC} \cdot SYN; \qquad DTA(0) = 0\end{aligned} \tag{3}$$

$$\begin{aligned}\frac{dSYN}{dt} = {} & k_{on-TC} \cdot DTA \cdot RTC_u - k_{off-TC} \cdot SYN + k_{on-TA} \\ & \cdot DTC \cdot RTA_u - k_{off-TA} \cdot SYN; \qquad SYN(0) = 0\end{aligned} \tag{4}$$

with k_{on} and k_{off} as the association and dissociation binding constants between MGD006 and the CD3 (TC) and CD123 (TA) receptors. These values were fixed to *in vitro* measured values (17). RTC_u and RTA_u represent the unbound molar concentrations of the CD3 and CD123 receptors, calculated on the basis of the total receptor concentrations (Supplementary Eq. S3).

Pharmacokinetic and ADA effect. The pharmacokinetic model describes the time-course of free drug plasma concentrations. MGD006 disposition was described by a two-compartment model, accounting for nonspecific drug distribution (tissue compartment), loss of drug due to ADA development, and loss of drug bound to CD3 or CD123 receptors with two target-mediated elimination pathways (22, 23). The effect of ADA development on MGD006 disposition was sorted into three groups: high, medium, and low effect. This categorization was based on the end of infusion concentrations in ADA-positive monkeys as compared with ADA-negative animals (Supplementary Fig. S3). Free MGD006 plasma concentration (C_{cen}) was described by the following equation;

$$\begin{aligned}\frac{dC_{cen}}{dt} = {} & \frac{Input}{V_{cen}} - \left(\frac{CL}{V_{cen}} + \frac{Q}{V_{cen}} + k_{ADA}\right) \cdot C_{cen} + \frac{Q}{V_{per}} \cdot \frac{A_{per}}{V_{cen}} \\ & - k_{on-TC} \cdot C_{cen} \cdot RTC_u + k_{off-TC} \cdot DTC - k_{on-TA} \cdot C_{cen} \\ & \cdot RTA_u + k_{off-TA} \cdot DTA; \quad C_{cen}(0) = 0\end{aligned} \tag{5}$$

with V_{cen} and CL as the plasma volume of distribution and systemic clearance, A_{per} and V_{per} represent the amount of drug and volume of distribution of the peripheral tissue compartment, and Q is the intercompartmental distribution clearance (Supplementary Eq. S4). The *Input* term represents dose administration and k_{ADA} is the first-order elimination rate constant due to ADA development (Supplementary Eq. S5).

Total T-cell dynamics. Total T-cell counts were modeled as the combination of two T-lymphocyte populations: (i) circulating T cells, which undergo trafficking and bind to the drug, and

(ii) activated T cells, produced following the synapse formation. Predicted concentrations of the MGD006/CD3 complex were used as a driver for T-cell redistribution, which was characterized by an indirect response model (24):

$$\frac{dTC}{dt} = k_{in-TC}(t) \cdot AF_{TC}^{\gamma} \cdot \left(1 - I_{max} \cdot \frac{DTC}{IC_{50} + DTC}\right) - k_{out-TC} \cdot TC; \quad (6)$$

$$TC(0) = \frac{k_{in-TC}(0)}{k_{out-TC}}$$

with TC representing the T-cell count in plasma, $k_{out\text{-}TC}$ is a first-order degradation rate constant, and $k_{in\text{-}TC}$ is the apparent zero-order production rate of T cells. T cells exhibited a greater baseline after the end of treatment. Therefore, $k_{in\text{-}TC}$ was modeled as a time-dependent change parameter, which increases to a new value, k_{inTC}^{ss}, after a lag time ($Tlag$), via a first-order logistic growth rate constant, k_d (Supplementary Eq. S6). I_{max} is the maximal fold inhibition of k_{inTC}, and IC_{50} is the plasma MGD006/CD3 complex concentration producing half-maximal inhibition of $k_{in\text{-}TC}$. After drug elimination, T-cell counts increased beyond the initial baseline, thus an adaptive feedback process (AF_{TC}) was included (25), as defined by Supplementary Eq. S6.

The activated T-cell population was defined by a virtual compartment, which represents the number of T cells getting activated (vATC) due to the binding of MGD006 to CD3 and CD123 receptors. Thus, prior to drug administration, it is assumed that no vATC is present in the system. The following analytic equation was used to describe vATC dynamics:

$$vATC(t) = \begin{cases} 0 & if\ TAD = 0 \\ \propto \cdot SYN + k_{prol} \cdot (1 - e^{-\beta \cdot TAD}) & if\ 0 < TAD \le T_P \\ \propto \cdot SYN + k_{prol} \cdot (1 - e^{-\beta \cdot T_P}) \cdot e^{-\beta(TAD - T_P)} & if\ TAD > T_P \end{cases} \quad (7)$$

vATC proliferation is driven by two components. vATC increases in response to the formation of the synapse, and T-cell differentiation was induced by the trimolecular complex concentrations multiplied by a stimulation factor α (without a time delay). Once, T cells are activated, they enter a phase of rapid cell division, which would be limited in time and independent of the complex concentrations (26). The clonal expansion phase of vATC was defined using an infusion-type equation, defined by TAD, k_{prol}, β, and T_p. TAD is a new time scale accounting for the delay at which vATC can start to renew, T_p represents the time window of the self-proliferation capacity of vATC, k_{prol} denotes the stimulation factor of vATC self-proliferation, and β is the vATC exponential growth rate constant. Studies show that T-cell activation is strictly dependent on the presence of MGD006 and both T cells and CD123$^+$ cells. Thus, the clonal expansion phase was conditionally included in the model, used only following synapse-mediated T-cell activation. The total T-cell counts were obtained by the sum of the TC and vATC pools (Supplementary Eq. S8).

CD123$^+$ cell dynamics. The virtual pool of vATC was used to drive the peripheral depletion of CD123$^+$ cells, rather than the trimolecular complex concentrations. Similarly to T-cell dynamics, an indirect response model with adaptive feedback was used to define the rate of change of CD123$^+$ cells:

$$\frac{dTA}{dt} = k_{in-TA} \cdot AF_{TA}^{\$} - k_{out-TA} \cdot TA - k_k \cdot vATC \cdot TA; \qquad TA(0) = \frac{k_{in-TA}}{k_{out-TA}} \quad (8)$$

with TA representing the CD123$^+$ cell counts in plasma, $k_{in\text{-}TA}$ is the zero-order production rate constant, and $k_{out\text{-}TA}$ is the first-order removal rate constant of CD123$^+$-cells. k_k is the second-order depletion rate constant of CD123$^+$-cells from plasma, and AF_{TA} is the adaptive feedback process of CD123$^+$ cells, defined by an adaptive feedback rate constant and power coefficient (Supplementary Eq. S9).

Statistical analysis. Drug exposure, total T cells, and CD123$^+$ cell dynamics were analyzed in a sequential manner using a population-based approach, which focuses on characterizing the variability among individuals within a target population (27). Each model parameter is defined by a typical value and by its variability within the subject population. Model parameters were estimated with the Stochastic Approximation Expectation Maximization algorithm in Monolix (version 4.32; http://www.lixoft.com/). Data from the animal groups receiving continuous 4-day infusions (groups 2–5) were used for model development, whereas data from group 6 (receiving continuous 7-day infusions) were used for model validation. Additional details are provided in Supplemental Materials (Section 1). Model selection was based upon diagnostic plots, precision of parameter estimates (relative standard error), and changes in the value of the objective function. Internal validation was performed using a prediction-corrected visual predictive check (PC-VPC; ref. 28). Five hundred replicates of the analysis dataset were simulated. The raw data were overlaid on the 5th, 50th, and 95th percentiles of the simulations to visually assess concordance between the observations and the model-based simulated data. In addition, external model validation was performed by VPC with the simulated 7-day infusion dosing schedule (group 6) compared with observed data (Berkeley-Madonna 8.3).

Results

The observed pharmacokinetic and pharmacodynamic profiles are shown in Fig. 2. During the first week, following vehicle control administration, no change in the profiles was observed. Following each drug infusion, MGD006 concentrations were rapidly eliminated from plasma. The impact of ADA development on MGD006 disposition was highly variable between animals. Total T-cell dynamics displayed a trafficking pattern after each dose administration. T-cell counts rapidly decreased during drug infusion and then increased slightly above initial values (i.e., rebound) once MGD006 was eliminated from the system. Following treatment, total T-cell counts were maintained at a higher baseline, as compared with the initial observed count prior to treatment. CD123$^+$ cells count exhibited a strong depletion after the first drug administration with the lower dose (100 ng/kg/day) in all animals; however, the duration of this depletion was highly variable. For some animals, CD123$^+$ cell counts stayed low until the end of the study, whereas for others, counts started to increase following the end of treatment. Some rebounds beyond the baseline were also observed. All of the observed profiles showed high inter-individual variability (IIV).

ADA categorization

Anti-drug antibodies developed in 23 of 32 monkeys during the study, which were detected before the start of the third (day 22) or the fourth infusion (day 29). These animals were categorized into different groups according to the time of

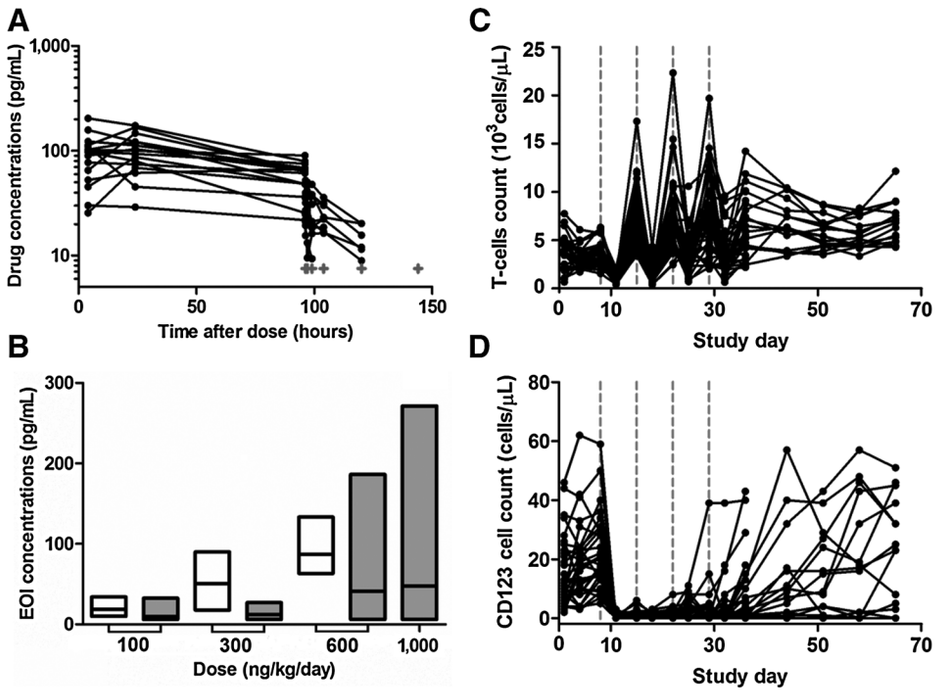

Figure 2.
Observed MGD006 pharmacokinetic/pharmacodynamic profiles. **A,** The MGD006 dose-normalized concentrations as a function of time for animal groups 3 and 4 at the doses of 300 and 600 ng/kg/day. **B** (bottom left) shows the end of infusion (EOI) MGD006 concentrations for each dose, for animals without (white boxplot) and with (gray boxplot) anti-drug antibodies. Each boxplot represents the minimum, maximum, and mean values. **C** (top right), The time-course of the total T-cell counts. **D** (bottom right), the time-course of $CD123^+$ cell counts. **B–D,** Data from all animals receiving continuous 4-day infusions (groups 2–5). Each individual animal data are connected with a line in **A**, **C**, and **D**. In **C** and **D**, the vertical dotted lines represent the start of weekly 4-day continuous infusions of the drug.

appearance and defined effect level of ADA (Supplementary Table S1).

Pharmacokinetic/ADA model

The time courses of observed and predicted free MGD006 plasma concentrations for four representative monkeys, two with and without ADA, are shown in Fig. 3 (first row). All individual profiles are provided in Supplementary Fig. S4. The disposition of MGD006 was best described by a two-compartment model with linear and target-mediated elimination pathways. The effect of ADA development was included as an additional elimination pathway, with one rate constant for each defined ADA effect. Estimated population pharmacokinetic parameters, along with interindividual variability and residual error are reported in Table 1. All parameters were estimated with good precision. The central volume of distribution was fixed to the physiological blood volume of cynomolgus monkeys, 65 mL/kg, multiplied by the weight for each animal (29). Terminal half-life for MGD006 was estimated at 3.5 hours. The "low" ADA elimination rate constant was set to zero, as no significant impact on MGD006 concentrations was identified. The "high" ADA elimination rate constant was fixed to a high empirical value via local sensitivity analysis (data not shown) to describe the decrease in drug concentrations below the LOQ. The pharmacokinetic model included the binding of MGD006 to CD3 and CD123 with respective association ($k_{on\text{-}TC}$, $k_{on\text{-}TA}$) and dissociation ($k_{off\text{-}TC}$, $k_{off\text{-}TA}$) rate constants. The ratio of these constants (k_{off}/k_{on}) define the equilibrium dissociation constants for CD3 and CD123 (9.2 and 0.27 nmol/L), suggesting that the drug preferentially binds to $CD123^+$ cells. The model-fitted curves captured the data well, and model diagnostic plots are provided in Supplementary Figs. S7 and S8, showing no systematic bias. The external validation is shown in Fig. 4 for two representative animals, one with and without ADA formation, and all individual profiles are provided in Supplementary Fig. S9. The model was able to reproduce the drug concentration–time profiles after continuous 7-day infusions.

Total T-cell model

The time-course of the total T-cell counts was described by the combination of two models representing lymphocyte dynamics and the production of activated T cells. Observed and predicted total T-cell counts are shown in Fig. 3 (third row) and Supplementary Fig. S5, and all estimated parameters are reported in Table 1.

Lymphocytes exhibited dose-dependent cell trafficking, which was captured by an indirect response model with an adaptive feedback process. T-cell redistribution was driven by the predicted MGD006/CD3 complex concentrations, which are displayed in Fig. 3 (second row). I_{max} was fixed to 100%, and the IC_{50} was estimated to be 1.18×10^{-3} pmol/L (IIV 155%), which confirms a potent inhibition by the MGD006/CD3 complex. ADA development with medium or high effect resulted in a decrease of MGD006 concentrations, leading to clear perturbations and/or diminution of T-cell trafficking. A logistic time-dependent change $k_{in\text{-}TC}$ was modeled to capture the higher baseline T-cell values following treatment. After a delay, fixed to 72 hours after drug administration, $k_{in\text{-}TC}$ increased to a new production rate, such that following drug treatment, T-cell counts were increased by 1.83-fold (±0.35).

The activated T-cell population was described using a virtual compartment. Predicted trimolecular complex concentrations were used to drive the production of vATC (Fig. 3, fourth row). The stimulation factor α was estimated at 2.1×10^6 cells/pmol and was associated with a high IIV of 194%. vATC clonal expansion started after a delay (fixed to 72 hours) and was defined by k_{prol} and β, estimated at 8.90 cells/μL and 7.13×10^{-3} per hour. The duration of the self-replication, T_p, was estimated at 17 days

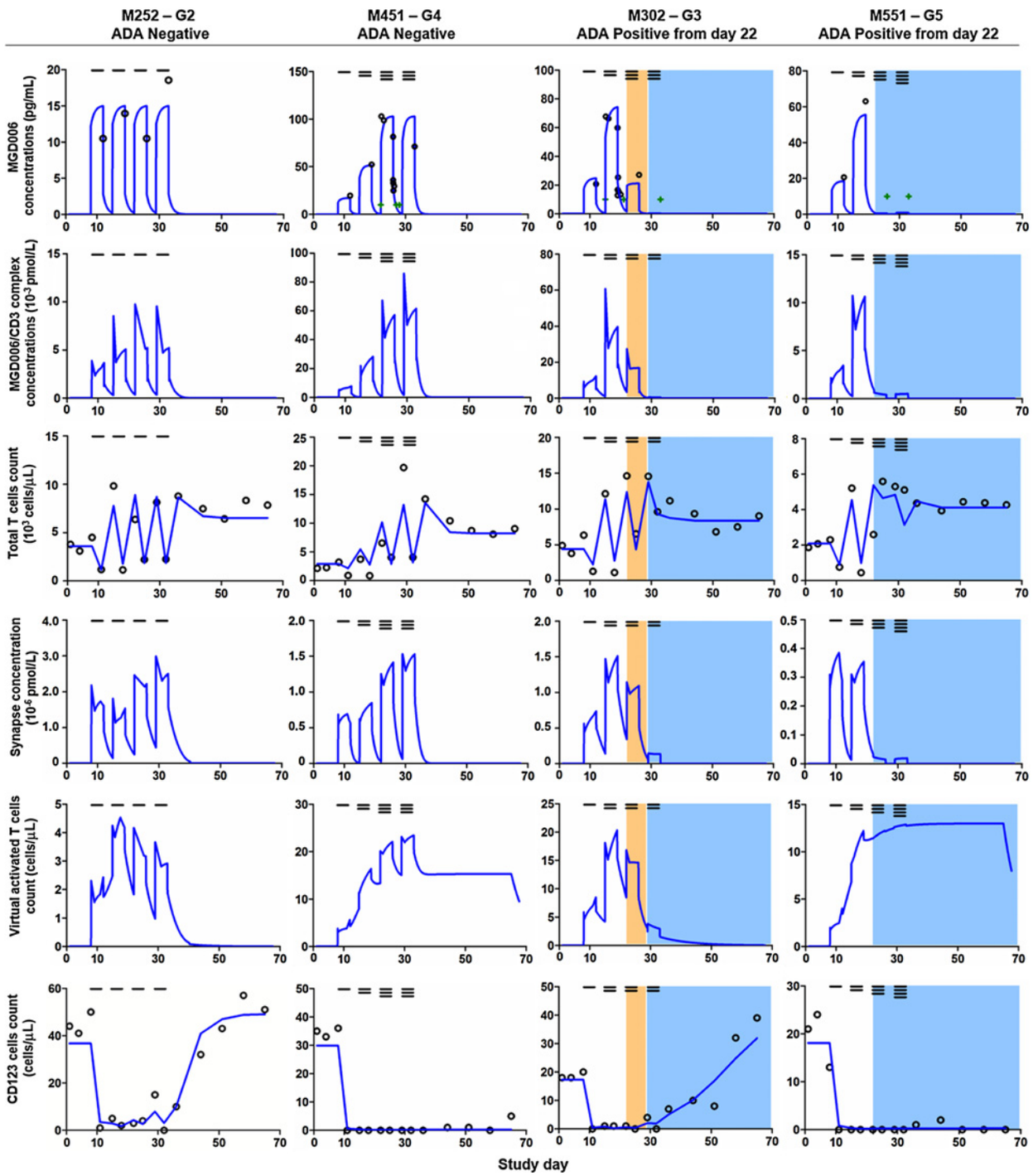

Figure 3.

Individual profiles for four representative cynomolgus monkeys receiving continuous 4-day MGD006 infusions. Drug concentrations (first row), MGD006/CD3 complex concentrations (second row), total T-cell counts (third row), MGD006/CD3/CD123 synapse concentrations (fourth row), virtual activated T-cell counts (fifth row), and $CD123^{+}$ cell counts (sixth row). Circles represent the observed data. Solid blue lines are the individual model predictions. Horizontal black lines represent the dose at each administration (1–100; 2–300; 3–600; 4–1,000 ng/kg/day). M_N and G_N represent the animal and group identification. The shaded background indicates the presence of anti-drug antibodies (ADA): orange for ADA with medium effect and blue for ADA with high effect.

Table 1. Pharmacokinetic/pharmacodynamic model parameter estimates for MGD006 in cynomolgus monkeys

Parameter (unit)	Definition	Estimate (RSE,%)	IIV[a] (RSE,%)
PK/ADA model			
V_{cen}, L/kg	Central volume of distribution	0.065 (-)	NE
CL, L/h	Central clearance	0.707 (5.0)	23.7 (12)
V_{per}, L	Peripheral volume of distribution	4.38 (7.0)	16.6 (32)
Q, L/h	Peripheral clearance	0.233 (9.0)	34.2 (19)
k_{1ADA}, per hour	High ADA elimination rate constant	800 (-)	NE
k_{2ADA}, per hour	Medium ADA elimination rate constant	8.94 (31)	81.1 (30)
$\varepsilon_{prop\text{-}DART}$, -	MGD006 residual proportional error	0.381 (6.0)	NE
Total T-cell model			
$k_{on\text{-}TC}$, L/pmol/h	MGD006/CD3 association constant	1.98×10^{-3} (-)	NE
$k_{off\text{-}TC}$, per hour	MGD006/CD3 dissociation constant	18 (-)	NE
Base, cells/μL/h	Central T-cell baseline	3.07×10^{3} (4.0)	10.6 (45)
$k^{ss}_{in\text{-}TC}$, cells/μL/h	Increased production rate constant	1.39×10^{4} (15)	53.5 (37)
k_d, per hour	Logistic growth rate constant	1.26×10^{-2} (20)	62.9 (48)
$k_{out\text{-}TC}$, per hour	First-order degradation rate constant	0.962 (5.0)	29.0 (13)
I_{max}, -	Maximum inhibition factor	1.00 (-)	NE
IC_{50}, pmol/L	MGD006 concentration inducing 50% of k_{in}	1.18×10^{-3} (31)	155 (14)
$k_{t\text{-}TC}$, -	Adaptive feedback rate constant	9.18×10^{-3} (18)	37.9 (56)
γ, -	Adaptive feedback power coefficient	1.66 (7.0)	16.6 (44)
α, 10^6 cells/pmol	Stimulation factor of vATC production	2.1 (35)	194 (13)
k_{prol}, cells/μL	vATC clonal expansion factor	8.90 (19)	64.7 (28)
β, per hour	vATC exponential growth rate constant	7.13×10^{-3} (22)	81.8 (23)
T_p, h	vATC clonal expansion duration	411 (29)	122 (18)
$\varepsilon_{prop\text{-}TC}$, -	T-cell residual proportional error	0.260 (4.0)	NE
$CD123^+$ cells model			
$k_{on\text{-}TA}$, L/pmol/h	MGD006/CD123 association constant	5.4×10^{-3} (-)	NE
$k_{off\text{-}TA}$, h	MGD006/CD123 dissociation constant	1.44 (-)	NE
$k_{in\text{-}TA}$, cells/μL/h	Zero-order production rate constant	5.54 (9.0)	41.6 (17)
$k_{out\text{-}TA}$, per hour	First-order degradation rate constant	0.356 (8.0)	36.1 (18)
k_k, μL/cell/h	Second-order CD123 depletion factor	2.17 (9.0)	43.2 (17)
$k_{t\text{-}TA}$, -	Adaptive feedback rate constant	2.55×10^{-4} (20)	74.5 (23)
δ, -	Adaptive feedback power coefficient	0.443 (25)	124 (15)
$\varepsilon_{add\text{-}CD123}$, cells/μL	CD123-cell residual additional error	0.987 (7.0)	NE
$\varepsilon_{prop\text{-}CD123}$, -	CD123-cell residual proportional error	0.312 (10)	NE

NOTE: Justification for fixed parameters can be found in Supplementary Materials (Section S1). Parameter shrinkage values, based on the variance of estimated individual random effects, were greater than 50% for V_{per}, k_{2ADA}, $k_{t\text{-}TC}$, γ, $k_{t\text{-}TA}$, k_{prol}, β, and k_k. All other parameters showed shrinkages below 40%–50%; equivalent to 20%–30% of standard-deviation, which are the limits suggested by Savic and Karlsson (44).

Abbreviations: RSE, relative standard error of estimate; IIV, inter-individual variability; ε_{prop}, proportional residual error; ε_{add}, additive resiudal variability; NE, not estimated; -, fixed.

[a]Estimates are the apparent coefficient of variation for the inter-individual variability (%).

(411 hours) with high IIV (4–54 days). Predicted vATC counts are shown in Fig. 3 (fifth row).

The model well captured the total T-cell profiles, all parameters were well estimated, and diagnostic plots show good model performance (Supplementary Figs. S7 and S8). The total T-cell profiles from group 6 (for external validation) were correctly reproduced within the 90% prediction interval in the visual predictive check (Fig. 4; Supplementary Fig. S10). In this validation group, MGD006 was constantly present in the plasma starting from day 8, which maintained the suppression of T-cell counts over the duration of treatment.

$CD123^+$ cell model

$CD123^+$ cell dynamics was best described with an indirect response model and an adaptive feedback process. The time-course of observed and predicted $CD123^+$ cell counts are shown in Fig. 3 (sixth row) and Supplementary Fig. S6. All estimated parameters are reported in Table 1.

Predicted vATC counts were used to drive the peripheral depletion of $CD123^+$ cells with an estimated second-order rate factor, k_k, of 2.17 μL/cell/hour. As shown in Fig. 3, $CD123^+$ cells exhibit either a return to baseline or continued suppression following treatment, and the profiles appear independent of the presence of ADA (which decrease MGD006 concentrations) and the trimolecular complex concentrations. In contrast to the total T-cell dynamics, ADA development does not appear to be associated with clear trends in $CD123^+$ cell depletion.

The proliferation of the vATC pool, which is independent of synapse concentrations, provides a driving function for the peripheral depletion of $CD123^+$ cells when MGD006 concentrations are decreased owing to ADA development. An adaptive feedback process was necessary to capture instances of rebound above the baseline following treatment. A power coefficient, estimated at 0.443 with a high IIV of 124%, significantly improved model fitting criteria.

The model-fitted curves well captured all of the $CD123^+$ cell profiles, and all model parameters were estimated with good precision. Model diagnostic plots suggested reasonable model performance (Supplementary Figs. S7 and S8). In addition, simulations of the $CD123^+$ cell profiles in the external validation group show that the model captured the data well (Fig. 4; Supplementary Fig. S11).

Discussion

CD123-targeted therapies for AML have generated considerable interest. Several drugs targeting CD123 are in development,

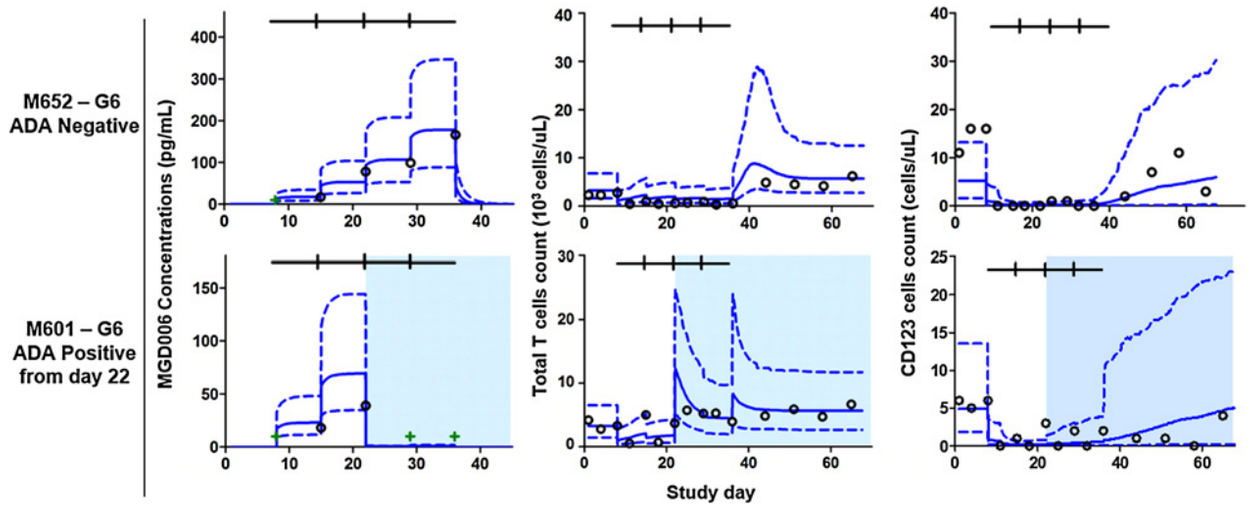

Figure 4.

Visual predictive checks (VPCs) of the pharmacokinetic/pharmacodynamic model predictions of MGD006 concentrations (left), total T-cell counts (center), and CD123$^+$cell counts (right), in two representative cynomolgus monkeys receiving continuous 7-day infusions. Circles represent the observed data. Green crosses are the drug concentrations below the limit of quantification. Solid blue lines represent the median of 500 model-simulated animal profiles. Dashed blue lines represent the 5th and 95th percentiles of the simulations. Horizontal black lines show the continuous 7-day infusions with escalating doses (100-300-600-1,000 ng/kg/day). M_N and G_N represent the animal and group identification. The blue shaded background indicates the presence of anti-drug antibodies (ADAs) with high effect.

including CSL362, a second-generation anti-CD123 antibody engineered for optimal antibody-dependent cell-mediated cytotoxicity (21), and immunotherapy using modified T cells that express chimeric antigen receptors (30). In this analysis, a population-based pharmacokinetic/pharmacodynamic model was developed to provide insights into the drug- and system-specific properties of a CD3xCD123 DART molecule designed for treating AML. Bispecific antibodies are gaining popularity for the development of cancer treatments; however, the stoichiometry between the drug and target ligands and the factors controlling drug disposition required for optimal efficacy is not well known. Limited examples of mechanistic pharmacokinetic/pharmacodynamic analysis are available in the literature (31, 32).

In cynomolgus monkeys, MGD006 disposition appears to be linear and stationary over the range of tested doses. The short estimated elimination half-life of MGD006 (3.5 hours), which is comparable with that of blinatumomab in humans (33), was expected based upon the drug structure. Similar to BiTE molecules, MGD006 is constructed from the fusion and recombination of single-chain variable fragments from two specific mAbs. The relatively small size, 58.9 kDa, results in fast elimination. To maintain adequate plasma concentrations, continuous intravenous infusion for several days is required. One strategy to overcome this issue is the addition of a human modified IgG1 Fc fragment to the bispecific molecule to increase the molecular weight and to take advantage of neonatal Fc receptor binding to achieve longer circulating half-life. PF-06671008, an Fc LP-DART molecule directed against P-cadherin and CD3, exhibited an extended half-life of approx. 4.4 days in human FcRn knock-in mice, whereas DART proteins usually exhibit half-lives less than 4 hours in several strains of mice (34).

Binding of MGD006 to both CD3 and CD123 was incorporated in the pharmacokinetic model as a target-mediated disposition process. For many mAbs, binding to the pharmacologic target influences their distribution and elimination, especially for those targeting membrane-bound antigens, and can result in nonlinear kinetics (35). For MGD006, target affinity and/or abundance were not high enough to have a significant influence on drug disposition. However, the incorporation of sequential binding in the model was an essential step to describe the mechanism of action of the bispecific antibody, as the starting point of its pharmacological activity is the formation of the synapse between MGD006, CD3, and CD123.

The differential impact of ADA development on T-lymphocyte and CD123$^+$ cell dynamics was an unexpected finding in this analysis. The concentration and reactivity of ADA can vary substantially from one monkey to another. Therefore, the heterogeneous nature of the MGD006 concentration–time profiles was anticipated, and monkeys were sorted in different ADA groups. The development of ADA with medium and/or high effect was associated with clear perturbations of T-cell trafficking, suggesting that T-cell redistribution is dependent on the presence of MGD006 in plasma. The decrease in T-cell counts likely represents cell migration toward tissues or an increased adhesion of the cells to blood vessels, triggered by the binding of the drug to CD3. The later increase in T-cell counts following MGD006 exposure is thought to be due to stimulation by subsequent cytokine release (19). Lymphocyte trafficking is a phenomenon that has been well described with an indirect pharmacokinetic/pharmacodynamic model following the administration of corticosteroids in humans (36, 37). Interestingly, the turnover of T-cell dynamics was modeled in cynomolgus monkeys following exposure to FTY720, another immunosuppressive agent, and the estimated system turnover parameters values ($k_{in\text{-}TC}$, $k_{out\text{-}TC}$) are similar to those estimated in this analysis (38).

In contrast to T cells, targeted CD123$^+$ cell dynamics was not apparently influenced by ADA development. CD123$^+$ cell depletion was effective in all animals receiving low doses, suggesting a

potent target activity of MGD006. However, the length of this depletion was highly variable and independent of ADA development. In a mechanistic *in vitro* pharmacokinetic/pharmacodynamic model developed for a P-Cadherin LP-DART molecule, the antitumor activity was modeled with a simple Hill function driven by the concentration of the trimolecular complex (31). However, using the synapse concentration as a driver for peripheral $CD123^+$ cell depletion with the same function would not have allowed for the apparent disconnect between the two types of profiles. One is for animals without ADA whose $CD123^+$ cells stay suppressed until the end of the study. Second is for animals that developed ADA-neutralizing MGD006 concentrations, but whose $CD123^+$ cells exhibited a late or no return to baseline following treatment. Targeted cell profiles suggest that the observed cell depletion could not be governed exclusively by the presence of the drug in plasma alone. Rather than synapse concentrations, T-cell activation following synapse formation was used to drive the pharmacological activity of MGD006 and successfully reconciled its pharmacokinetic/pharmacodynamic properties.

Activation of the immune system is a complex process that involves different types of T cells ($CD4^+$, $CD8^+$) with specific roles and activation pathways. MGD006 has been shown to generate *in vitro* and *in vivo* T-cell activation and expansion, independent of T-cell specificity. The factors regulating the clonal expansion of activated lymphocytes are not fully understood. Models have been developed to describe the population kinetics of T cells (with a predator-prey type modeling approach) based upon a proliferation of activated T cells and dependent on the continual presence of a specific antigen (39). Several studies have shown that this concept might be incomplete and suggest that activated T cells could also proliferate in an antigen-independent manner and be programmed within a certain time window (40, 41). The timing control of the antigen-independent proliferation is not known but could be determined by intracellular signals or externally by cytokines (26). A clonal expansion phase of T cells, with both antigen-dependent and independent components, has been included in the model with the trimolecular concentrations as the antigen. We have assumed that the decrease of MGD006 concentrations owing to ADA development does not prevent the vATC pool from proliferating in some monkeys. The equation used to describe the vATC count (Eq. 7) combined a stimulation factor linked to the trimolecular complex concentrations and an empirical function independent of the complex. This function allowed for vATC proliferation, and the intensity and duration of this function were estimated. Predicted vATC counts were very low compared with total T-cell counts, but these values should be carefully and quantitatively interpreted (e.g., model parameters) owing to the virtual nature of the compartment used to describe their dynamics and the sequential modeling approach. The binding of MGD006 to CD3 and CD123 led to two delayed effects: a prolonged T-cell expansion and greater T-cell baselines after treatment. Both effects were modeled using a time-delay following the physiological characteristics of a cytolytic synapse. Once naïve T cells become activated by foreign epitopes through antigen-presenting cells, they slowly enter a cell division phase and expand into a large clone of effector cells over the next 4–5 days (13, 26). The same delay was computed for both effects and fixed to 72 hours after a sensitivity analysis (data not shown). The greater T-cell baseline was assumed to result from T-cell activation and expansion but was modeled using an independent function. The vATC pool was implemented in the model to drive the antitarget activity and did not include the potential subpopulations that may have contributed to T-cell expansion without influencing $C123^+$ cells (e.g., memory T cells). For some animals, $CD123^+$ cells also exhibited higher baselines following treatment; however, the reasons for this phenomenon remain unclear.

Our mathematical model was developed with a population-based approach to characterize the variability of the pharmacokinetic/pharmacodynamic parameters within the animal subjects, which was expected to be high owing to the diverse nature of the observed profiles. The parameters controlling T-cell trafficking induced by the MGD006/CD3 complex (IC_{50}), the stimulation of vATC production (α), and the duration of vATC clonal expansion (T_p) were estimated with high IIV (>100%, Table 1), highlighting the variability of the pharmacological activity of MGD006 within the population. Several estimated parameters also presented with high shrinkage values (Table 1), which could limit the ability to identify important covariate relationships; however, this was not an objective of this preclinical study. High shrinkage was expected around the parameters defining the virtual pool of activated T cells as there are no data to back-up the estimates, but the inclusion of this pool was necessary to characterize the drug response in a mechanistic manner. CD3 and CD123 receptor burdens were calculated based upon receptor densities and number of specific cells. The densities of both receptors were fixed to a mean value and were assumed to be time invariant. However, the numbers of CD3 and CD123 receptors per cell may be highly variable, which would alter individual animal receptor concentrations and add variability to subsequent pharmacological effects. Moreover it has been shown that CD3 expression has a prominent influence on T-cell activation triggering (20). The future inclusion of individual subject receptor density could further explain the variability in pharmacodynamic parameters and the different responses to drug administration.

The final pharmacokinetic/pharmacodynamic model represents a mechanistic framework, through an integration of pharmacokinetic and pharmacological processes, and can be used to anticipate different dosing scenarios in patients with AML quantitatively. MGD006 binds to both monkey and human antigens with similar affinities, and the mechanisms and processes emulated by the model can be assumed to be conserved in humans. A common approach to the extrapolation of animal pharmacokinetic/pharmacodynamic models to humans is to use allometric principles for pharmacokinetic and turnover parameters, whereas pharmacologic terms are often assumed to be species independent (42). In terms of MGD006 pharmacokinetics, simulations showed that target abundance and/or affinities did not have substantial impact on drug disposition (data not shown). Therefore, the pharmacokinetic model can be scaled using classic allometric exponents (i.e., 0.75 and 1) for clearance and volume parameters. For the pharmacodynamic models, the cell turnover rate constants can be scaled with an allometric exponent of −0.25. The intrinsic capacity and sensitivity of the drug complexes (I_{max}, IC_{50}, k_k) may be assumed to be similar in humans. The parameters regulating the binding process (association/dissociation rate constant, CD3/CD123 receptor densities) that are known or defined in humans can be directly implemented in the model (17, 20, 21). The major difference in patients with AML is the effector-to-target cell ratio. Patients may exhibit lymphopenia and a greater pool of

$CD123^+$ blast cells compared with monkeys that only express normal blood $CD123^+$ cells. Therefore, the initial baseline of both cells may need to be adjusted. In the model, receptor concentrations are calculated based upon both the number of cells and receptor densities. The model has the flexibility to predict different scenarios in terms of the CD123 pool (i.e., patients with large/small numbers of blast cells and high/low receptor densities). ADA development is not expected in humans, but its impact can be simulated as well. More complex mathematical models developed for AML disease could also be integrated within this framework (43).

In summary, a mechanistic pharmacokinetic/pharmacodynamic model was developed to describe the disposition of a bispecific antibody, the dynamics of its targets, and the impact of its immunogenicity in cynomolgus monkeys. The model highlights the key role of T-cell activation and expansion following the trimolecular complex formation for antitarget cell activity and the variability that can be expected. The model was robust enough to predict a dosing regimen in monkeys that was not used in model development, and it may be useful for informing dosing strategies in humans.

Disclosure of Potential Conflicts of Interest

D.E. Mager reports receiving commercial research grants from Servier. No potential conflicts of interest were disclosed by the other authors.

Authors' Contributions

Conception and design: O. Campagne, A. Delmas, G.R. Chichili, R. Alderson
Development of methodology: O. Campagne, G.R. Chichili, H. Li, R. Alderson
Acquisition of data (provided animals, acquired and managed patients, provided facilities, etc.): G.R. Chichili, H. Li, R. Alderson
Analysis and interpretation of data (e.g., statistical analysis, biostatistics, computational analysis): O. Campagne, M. Chenel, G.R. Chichili, D.E. Mager
Writing, review, and/or revision of the manuscript: O. Campagne, A. Delmas, S. Fouliard, M. Chenel, G.R. Chichili, D.E. Mager
Administrative, technical, or material support (i.e., reporting or organizing data, constructing databases):
Study supervision: A. Delmas, S. Fouliard, J.-M. Scherrmann, D.E. Mager

Acknowledgments

The authors would like to thank Marie-Hélène Brillanceau from Institut de Recherches Internationales Servier for her support coordinating the transfer of information between MacroGenics and Institut de Recherches Internationales Servier. This work was incorporated into a PhD project (Olivia Campagne), granted by the Institut de Recherches Internationales Servier.

The costs of publication of this article were defrayed in part by the payment of page charges. This article must therefore be hereby marked *advertisement* in accordance with 18 U.S.C. Section 1734 solely to indicate this fact.

Received August 6, 2017; revised October 3, 2017; accepted February 15, 2018; published OnlineFirst February 20, 2018.

References

1. Estey E, Döhner H. Acute myeloid leukaemia. Lancet 2006;368:1894–907.
2. Dohner H, Estey EH, Amadori S, Appelbaum FR, Buchner T, Burnett AK, et al. Diagnosis and management of acute myeloid leukemia in adults: recommendations from an international expert panel, on behalf of the European LeukemiaNet. Blood 2010;115:453–74.
3. Estey EH. Acute myeloid leukemia: 2014 update on risk-stratification and management. Am J Hematol 2014;89:1063–81.
4. American Cancer Society. Cancer facts & figures 2016. Atlanta, GA: American Cancer Society; 2017.
5. Ishikawa Y, Kiyoi H, Tsujimura A, Miyawaki S, Miyazaki Y, Kuriyama K, et al. Comprehensive analysis of cooperative gene mutations between class I and class II in de novo acute myeloid leukemia. Eur J Haematol 2009;83:90–8.
6. Baeuerle PA, Reinhardt C. Bispecific T-cell engaging antibodies for cancer therapy. Cancer Res 2009;69:4941–4.
7. Riethmuller G. Symmetry breaking: bispecific antibodies, the beginnings, and 50 years on. Cancer Immun 2012;12:12.
8. Kontermann RE, Brinkmann U. Bispecific antibodies. Drug Discov Today 2015;20:838–47.
9. Wu J, Fu J, Zhang M, Liu D. Blinatumomab: a bispecific T cell engager (BiTE) antibody against CD19/CD3 for refractory acute lymphoid leukemia. J Hematol Oncol 2015;8:104.
10. Clevers H, Alarcon B, Wileman T, Terhorst C. The T cell receptor/CD3 complex: a dynamic protein ensemble. Annu Rev Immunol 1988;6:629–62.
11. Wolf E, Hofmeister R, Kufer P, Schlereth B, Baeuerle PA. BiTEs: bispecific antibody constructs with unique anti-tumor activity. Drug Discov Today 2005;10:1237–44.
12. Nagorsen D, Kufer P, Baeuerle PA, Bargou R. Blinatumomab: a historical perspective. Pharmacol Ther 2012;136:334–42.
13. de la Roche M, Asano Y, Griffiths GM. Origins of the cytolytic synapse. Nat Rev Immunol 2016;16:421–32.
14. Moore PA, Zhang W, Rainey GJ, Burke S, Li H, Huang L, et al. Application of dual affinity retargeting molecules to achieve optimal redirected T-cell killing of B-cell lymphoma. Blood 2011;117:4542–51.
15. Jordan CT, Upchurch D, Szilvassy SJ, Guzman ML, Howard DS, Pettigrew AL, et al. The interleukin-3 receptor alpha chain is a unique marker for human acute myelogenous leukemia stem cells. Leukemia 2000;14:1777–84.
16. Testa U, Riccioni R, Militi S, Coccia E, Stellacci E, Samoggia P, et al. Elevated expression of IL-3Ralpha in acute myelogenous leukemia is associated with enhanced blast proliferation, increased cellularity, and poor prognosis. Blood 2002;100:2980–8.
17. Chichili GR, Huang L, Li H, Burke S, He L, Tang Q, et al. A CD3xCD123 bispecific DART for redirecting host T cells to myelogenous leukemia: preclinical activity and safety in nonhuman primates. Sci Transl Med 2015;7:289ra82.
18. Al-Hussaini M, Rettig MP, Ritchey JK, Karpova D, Uy GL, Eissenberg LG, et al. Targeting CD123 in acute myeloid leukemia using a T-cell–directed dual-affinity retargeting platform. Blood 2016;1:122–31.
19. May MB, Glode A. Blinatumomab: a novel, bispecific, T-cell engaging antibody. Am J Health Syst Pharm 2016;73:e6–e13.
20. El Hentati FZ, Gruy F, Iobagiu C, Lambert C. Variability of CD3 membrane expression and T cell activation capacity. Cytometry B Clin Cytom 2010;78:105–14.
21. Busfield SJ, Biondo M, Wong M, Ramshaw HS, Lee EM, Ghosh S, et al. Targeting of acute myeloid leukemia in vitro and in vivo with an anti-CD123 mAb engineered for optimal ADCC. Leukemia 2014;28:2213–21.
22. Mager DE, Jusko WJ. General pharmacokinetic model for drugs exhibiting target-mediated drug disposition. J Pharmacokinet Pharmacodyn 2001;28:507–32.
23. Gibiansky L, Gibiansky E. Target-mediated drug disposition model for drugs that bind to more than one target. J Pharmacokinet Pharmacodyn 2010;37:323–46.
24. Jusko WJ, Ko HC. Physiologic indirect response models characterize diverse types of pharmacodynamic effects. Clin Pharmacol Ther 1994;56:406–19.
25. Karlsson MO, Anehall T, Friberg LE, Henningsson A, Kloft C, Sandstrom M, et al. Pharmacokinetic/pharmacodynamic modelling in oncological drug development. Basic Clin Pharmacol Toxicol 2005;96:206–11.
26. De Boer RJ, Perelson AS. Quantifying T lymphocyte turnover. J Theor Biol 2013;327:45–87.
27. Aarons L. Population pharmacokinetics: theory and practice. Br J Clin Pharmacol 1991;32:669–70.

28. Bergstrand M, Hooker AC, Wallin JE, Karlsson MO. Prediction-corrected visual predictive checks for diagnosing nonlinear mixed-effects models. AAPS J 2011;13:143–51.
29. Diehl KH, Hull R, Morton D, Pfister R, Rabemampianina Y, Smith D, et al. A good practice guide to the administration of substances and removal of blood, including routes and volumes. J Appl Toxicol 2001;21:15–23.
30. Pizzitola I, Anjos-Afonso F, Rouault-Pierre K, Lassailly F, Tettamanti S, Spinelli O, et al. Chimeric antigen receptors against CD33/CD123 antigens efficiently target primary acute myeloid leukemia cells in vivo. Leukemia 2014;28:1596–605.
31. Chen X, Haddish-Berhane N, Moore P, Clark T, Yang Y, Li H, et al. Mechanistic projection of first-in-human dose for bispecific immunomodulatory P-Cadherin LP-DART: An integrated PK/PD modeling approach. Clin Pharmacol Ther 2016;100:232–41.
32. Gadkar K, Yadav DB, Zuchero JY, Couch JA, Kanodia J, Kenrick MK, et al. Mathematical PKPD and safety model of bispecific TfR/BACE1 antibodies for the optimization of antibody uptake in brain. Eur J Pharm Biopharm 2016;101:53–61.
33. Klinger M, Brandl C, Zugmaier G, Hijazi Y, Bargou RC, Topp MS, et al. Immunopharmacologic response of patients with B-lineage acute lymphoblastic leukemia to continuous infusion of T cell-engaging CD19/CD3-bispecific BiTE antibody blinatumomab. Blood 2012;119:6226–33.
34. Root AR, Cao W, Li B, LaPan P, Meade C, Sanford J, et al. Development of PF-06671008, a highly potent Anti-P-cadherin/Anti-CD3 bispecific DART molecule with extended Half-Life for the treatment of cancer. Antibodies 2016;5:6.
35. Dostalek M, Gardner I, Gurbaxani BM, Rose RH, Chetty M. Pharmacokinetics, pharmacodynamics and physiologically-based pharmacokinetic modelling of monoclonal antibodies. Clin Pharmacokinet 2013;52:83–124.
36. Hong Y, Mager DE, Blum RA, Jusko WJ. Population pharmacokinetic/pharmacodynamic modeling of systemic corticosteroid inhibition of whole blood lymphocytes: modeling interoccasion pharmacodynamic variability. Pharm Res 2007;24:1088–97.
37. Mager DE, Lin SX, Blum RA, Lates CD, Jusko WJ. Dose equivalency evaluation of major corticosteroids: pharmacokinetics and cell trafficking and cortisol dynamics. J Clin Pharmacol 2003;43:1216–27.
38. Li H, Meno-Tetang GML, Chiba K, Arima N, Heining P, Jusko William J. Pharmacokinetics and cell trafficking dynamics of 2-amino-2-[2-(4-octylphenyl)ethyl]propane-1,3-diol hydrochloride (FTY720) in cynomolgus monkeys after single oral and intravenous doses. J Pharmacol Exp Ther 2002;301:519–26.
39. Nowak MA, Bangham C. Population dynamics of immune responses to persistent viruses. Science 1996;272:74–9.
40. Antia R, Ganusov VV, Ahmed R. The role of models in understanding CD8+ T-cell memory. Nat Rev Immunol 2005;5:101–11.
41. Antia R, Bergstrom CT, Pilyugin SS, Kaech SM, Ahmed R. Models of CD8+ responses: 1. What is the antigen-independent proliferation program. J Theor Biol 2003;221:585–98.
42. Mager DE, Jusko WJ. Development of translational pharmacokinetic-pharmacodynamic models. Clin Pharmacol Ther 2008;83:909–12.
43. Stiehl T, Baran N, Ho AD, Marciniak-Czochra A. Cell division patterns in acute myeloid leukemia stem-like cells determine clinical course: a model to predict patient survival. Cancer Res 2015;75:940–9.
44. Savic R, Karlsson MO. Importance of shrinkage in empirical bayes estimates for diagnostics: problems and solutions. AAPS J 2009;11:558–69.